SPH modelling of consolidation problem based on two-phase mixture theory

Hao Wu[1], Jinjian Chen[1], Chencong Liao[1], Jianhua Wang[1], Jian Wang[2]

[1]Department of civil engineering,
Shanghai Jiao Tong University, P.R.China
[2]Department of Water Conservancy and Hydropower Engineering,
Hohai University, P.R.China
Corresponding author: chulizi_hhu@hotmail.com

Abstract

The SPH based two-phase mixture model was improved by taking the soil porosity into account. The soil porosity was treated as a spatial variable but not a constant. A servo-control method was developed to model the stress boundary condition based on the frictional sliding contact algorithm. Then a 2-D consolidation numerical analysis was conducted to validate the ability of the SPH based two-phase model to predict the pore water pressure. Comparison with previous research proved that the SPH based two-phase mixture could capture the pore water pressure satisfactorily. In addition, the servo-control method could model the stress boundary condition well.

Keywords: SPH; Porosity; Two-phase mixture; Pore water pressure; Servo-control

1. Introduction

The well-known Biot-Zienkiewicz consolidation theory has been widely applied to consolidation and seepage problems in geotechnical engineering field [1]. Generally speaking, the Biot-Zienkiewicz theory focus on the soil deformation or the stationary state. The acceleration of the fluid phase is ignored and the soil-water interaction is taken into account implicitly. Few attention was paid to the flow process or the interaction between pure water region and the mixture. Therefore, the Biot-Zienkiewicz theory was rarely reported on studying the fast flows through high permeable porous media such as piping and scouring. By contrast, the two-phase mixture theory [2], in which soil and water are assumed to occupy part of the macroscopic mixture, is suitable for dealing with these problems. In the two-phase mixture theory, the soil and water satisfy their own governing equations and the interaction force is composed of pore water pressure and viscous drag force. Hence, not only the soil-water interaction within the mixture but also the interaction between the pure fluid region and the mixture could be investigated. Detailed theoretically comparison between the mixture theory and the Biot-Zienkiewicz theory could be found in Coussy [3].

Although extremely large soil deformation has been encountered when solving the abovementioned problems, smoothed particle dynamics (SPH) has been utilized to avoid the mesh distortion [4]. Recently, an amount of numerical studies has been reported on problems involving fast flow through porous media [5] and large soil deformation using SPH. Typical examples include saturated soil excavation by water jet [6, 7] and liquefaction problems [8–10]. However, the applicability of the SPH based two-phase mixture model has not been sufficiently validated. The most troublesome one is the ability to predict the pore water pressure. Different from the Biot-Zienkiewicz theory, in the two-phase mixture theory, the conservation equations of fluid phase are solved separately but not combined to the soil phase. The pore water pressure is in fact calculated through density variation. In this study, the ability of the SPH based two-phase mixture to capture the pore water pressure is validated through a classical 2-D consolidation problem. In addition, the original SPH mixture model was improved by considering the effect of the porosity. Besides, a servo-control algorithm has been developed to model the stress boundary condition. It is proved that the SPH based two-phase model could also predict the pore water pressure satisfactorily and the servo-control method could model the stress boundary condition well.

2. SPH background

In SPH, the computation domain is discretized by a finite number of particles, which carry field variables and material properties [11–13]. All the field variables and functions are interpolated on the particles and governing equations could be solved. The final particle approximation form of function and its derivative are given by

$$\langle f(\boldsymbol{x}_i)\rangle = \sum_{j=1}^{N} \frac{m_j}{\rho_j} f(\boldsymbol{x}_j) W\left(\boldsymbol{x}_i - \boldsymbol{x}_j, h\right) \tag{1}$$

$$\langle \nabla \cdot f(\boldsymbol{x}_i)\rangle = -\sum_{j=1}^{N} \frac{m_j}{\rho_j} f(\boldsymbol{x}_j) \cdot \nabla_j W\left(\boldsymbol{x}_i - \boldsymbol{x}_j, h\right) \tag{2}$$

where i and j denote particles; N is the total number of neighbor particles; m is mass and ρ is the density; m_j/ρ_j actually gives the finite volume ΔV_j that originates in the infinitesimal volume $d\boldsymbol{x}'$. W is the kernel or smoothing function; h is the smoothing length defining the influence domain of W. Of the several proposed kernels, we apply here the Wendland type [14] for its accuracy and efficiency,

$$W(q,h) = \alpha_d \times \begin{cases} (1-q/2)^4 (2q+1), & 0 \le q \le 2, \\ 0, & q \ge 2 \end{cases} \tag{3}$$

where α_d is the normalizing factor, $\alpha_d = 7/4\pi h^2$ for 2-D problems; q is relative distance, $q = |\boldsymbol{x} - \boldsymbol{x}'|/h$.

3. Governing equations and SPH formulations

The two-phase mixture theory is based on the assumption that each constitute occupies part of the macroscopic mixture [2]. The mass conservations are given in the following Lagrangian forms

$$\frac{\mathrm{d}\rho_s}{\mathrm{d}t} = -\rho_s \nabla \cdot \boldsymbol{v}_s, \quad \rho_s = (1-n)\tilde{\rho}_s \tag{4}$$

$$\frac{\mathrm{d}\rho_f}{\mathrm{d}t} = -\rho_f \nabla \cdot \boldsymbol{v}_f, \quad \rho_f = n\tilde{\rho}_f \tag{5}$$

where n is the soil porosity; $\tilde{\rho}_s$ is the particle density of soil and $\tilde{\rho}_f$ is the intrinsic density of the water; ρ_s and ρ_f are the apparent density of soil and water, respectively; $\boldsymbol{v}_s$ and $\boldsymbol{v}_f$ are the spatially averaged velocity of soil and water, respectively. Assuming that the particle density of soil keeps unchanged, the governing equation for the soil porosity could be obtained by

$$\frac{\mathrm{d}n}{\mathrm{d}t} = (1-n)\nabla \cdot \boldsymbol{v}_s \tag{6}$$

It could be seen from equation (6) that the soil porosity was treated as a spatial and temporal field variable but not a constant. Hence, the effect of soil porosity on the mixture behavior could be considered. In contrast, the soil porosity was either neglected or treated as a constant in previous studies, which was not in accord with the reality.

The conservation equation of momentum are given as

$$\rho_s \frac{\mathrm{d}\boldsymbol{v}_s}{\mathrm{d}t} = \nabla \cdot \boldsymbol{\sigma}' - (1-n)\nabla \tilde{p}_f + \boldsymbol{f}_d + \rho_s \boldsymbol{g} \tag{7}$$

$$\rho_f \frac{\mathrm{d}\boldsymbol{v}_f}{\mathrm{d}t} = -\nabla\left(n\tilde{p}_f\right) + \tilde{p}_f \nabla n + \nabla \cdot \left(n\tilde{\boldsymbol{\tau}}_f\right) - \boldsymbol{f}_d + \rho_f \boldsymbol{g} \tag{8}$$

$$\boldsymbol{f}_d = \frac{n^2 \tilde{\rho}_f g\left(\boldsymbol{v}_f - \boldsymbol{v}_s\right)}{k} \tag{9}$$

$$\boldsymbol{\sigma} = \boldsymbol{\sigma}' - (1-n)\,\tilde{p}_f \boldsymbol{I} + n\tilde{\boldsymbol{\sigma}}_f \tag{10}$$

$$\tilde{\boldsymbol{\sigma}}_f = -\tilde{p}_f \boldsymbol{I} + \tilde{\boldsymbol{\tau}}_f \tag{11}$$

where $\boldsymbol{\sigma}$ is the total stress tensor decomposed based on the Terzaghi's concept of effect stress. $\boldsymbol{\sigma}'$ is the effective stress relating to the strain rate in the constitutive model for soil. $\tilde{p}_f$ and $\tilde{\boldsymbol{\tau}}_f$ are the pore water pressure and shear stress of water, respectively. $\boldsymbol{g}$ is the gravity acceleration. $\boldsymbol{f}_d$ is the viscous drag force calculated by Darcy's law. k is the hydraulic conductivity.

By applying the particle approximation formulation, equation (5)-(9) could be rewritten in the following SPH form,

$$\frac{\mathrm{d}\rho_a}{\mathrm{d}t} = \sum_{b=1}^{M} m_b \boldsymbol{v}_{ab} \cdot \nabla_a W_{ab} + \delta_f h_a c_f \sum_{b=1}^{M} \frac{m_b}{\rho_b} \Psi_{ab} \cdot \nabla_a W_{ab} \tag{12}$$

$$\frac{\mathrm{d}n_i}{\mathrm{d}t} = (1-n_i)\sum_{j=1}^{N} \frac{m_j}{\rho_j} \boldsymbol{v}_{ji} \cdot \nabla_i W_{ij} \tag{13}$$

$$\frac{\mathrm{d}\boldsymbol{v}_i}{\mathrm{d}t} = \sum_{j=1}^{N} m_j \left(\frac{\boldsymbol{\sigma}'_i}{\rho_i^2} + \frac{\boldsymbol{\sigma}'_j}{\rho_j^2} + \Pi_{ij}\right) \cdot \nabla_i W_{ij} - (1-n_i)\sum_{a=1}^{M} \frac{m_a}{\rho_a} \frac{\tilde{p}_a}{\rho_i} \nabla_i W_{ai} + \sum_{a=1}^{M} \frac{m_a}{\rho_a} \frac{\boldsymbol{f}_{ia}}{\rho_i} W_{ai} + \boldsymbol{g}_i \tag{14}$$

$$\begin{aligned}\frac{\mathrm{d}\boldsymbol{v}_a}{\mathrm{d}t} = &-\sum_{b=1}^{M} m_b \left(\frac{\tilde{p}_a n_a}{\rho_a^2} + \frac{\tilde{p}_b n_b}{\rho_b^2} + \Pi_{ab} + f_{ab}^{\vartheta}\left(R_a + R_b\right)\right) \nabla_a W_{ab} + \sum_{b=1}^{M} m_b \left(\frac{\boldsymbol{\tau}_a n_a}{\rho_a^2} + \frac{\boldsymbol{\tau}_b n_b}{\rho_b^2}\right) \cdot \nabla_a W_{ab} \\ &+ \sum_{i=1}^{N} \frac{m_i}{\rho_i} \frac{\tilde{p}_a}{\rho_a} n_i \nabla_a W_{ai} - \sum_{i=1}^{N} \frac{m_i}{\rho_i} \frac{\boldsymbol{f}_{ia}}{\rho_a} W_{ai} + \boldsymbol{g}_a\end{aligned} \tag{15}$$

$$\boldsymbol{f}_{ia} = \frac{n_a^2 \tilde{\rho}_f g\left(\boldsymbol{v}_a - \boldsymbol{v}_i\right)}{k} \tag{16}$$

where i , j denote soil particles and a , b denote water particles. $\boldsymbol{v}_{ab} = \boldsymbol{v}_a - \boldsymbol{v}_b$, $\boldsymbol{v}_{ji} = \boldsymbol{v}_j - \boldsymbol{v}_i$. The second term on the right side of equation (12) is added to avoid density fluctuation and to obtain accurate pore water pressure, which is based on the $\delta - SPH$ method [15]. $\Psi_{ab} = 2(\rho_a - \rho_b)\frac{\boldsymbol{x}_{ab}}{\left|\boldsymbol{x}_{ab}\right|^2}$. δ_f is a constant normally set to 0.1, c_f is the sound speed of water. Π_{ij} and Π_{ab} are Monaghan-type artificial viscosity [16] used to remove unphysical penetration, defined as

$$\Pi_{ij} = \begin{cases} \dfrac{-\alpha_\Pi c_{ij}\Phi_{ij} + \beta_\Pi \Phi_{ij}^2}{\rho_{ij}}, & \boldsymbol{v}_{ij} \cdot \boldsymbol{x}_{ij} < 0 \\ 0, & \boldsymbol{v}_{ij} \cdot \boldsymbol{x}_{ij} \geq 0 \end{cases} \tag{17}$$

$$\Phi_{ij} = \frac{h_{ij}\boldsymbol{v}_{ij} \cdot \boldsymbol{x}_{ij}}{\left|x_{ij}\right|^2 + 0.01h_{ij}^2} \tag{18}$$

$$c_{ij} = \frac{c_i + c_j}{2}, \rho_{ij} = \frac{\rho_i + \rho_j}{2}, h_{ij} = \frac{h_i + h_j}{2} \tag{19}$$

Π_{ab} could be obtained by simply replace i, j with a, b. α_Π and β_Π are respectively set to 0.1 and 1.0 for soil, while for water take values of 0.01 and 1.0.

In this research, serious tensile instability was observed in low permeable soil. The artificial pressure method proposed by Monaghan [17] has been adopted throughout this study, i.e. the term $f_{ab}^{\vartheta}\left(R_a + R_b\right)$. f_{ab} is the repulsive term and specified by $f_{ab} = \frac{W_{ab}}{W\left(\Delta d, h\right)}$. Δd denotes the initial particle spacing, ϑ is usually taken as $W\left(0,h\right)/W\left(\Delta d,h\right)$. For Wendland kernel, n has the value about 3.24 with h equals to $1.2\Delta d$. The factor R_a and R_b are determined in terms of pressure,

$$R_a = \begin{cases} \dfrac{\ell\left|\tilde{p}_a\right|}{\rho_a^2}, & \text{if } \tilde{p}_a < 0 \\ 0, & \text{otherwise} \end{cases} \tag{20}$$

where ℓ is a small constant and typically taken as 0.2; R_b is calculated analogously.

To close the above equations, constitutive models are needed to determine $\boldsymbol{\sigma}'$, $\tilde{p}_f$, $\tilde{\boldsymbol{\tau}}_f$. In order to keep consistent with the results to be compared in Boer et al. [18] and Breuer [19] , an elastic constitutive relationship is adopted. The water is considered as weakly compressible Newtonian fluid. The final SPH discretized constitutive model for soil and water are given as follows.

For soil,

$$\dot{\sigma}_i'^{\alpha\beta} = 2G\dot{e}_i^{\alpha\beta} + K\dot{\varepsilon}_i^{\gamma\gamma}\delta_i^{\alpha\beta} \tag{21}$$

$$\dot{\varepsilon}_i^{\alpha\beta} = \frac{1}{2}\left(\sum_{j=1}^{N}\frac{m_j}{\rho_j}v_{ji}^{\alpha}\frac{\partial W_{ij}}{\partial x_i^{\beta}} + \sum_{j=1}^{N}\frac{m_j}{\rho_j}v_{ji}^{\beta}\frac{\partial W_{ij}}{\partial x_i^{\alpha}}\right) \tag{22}$$

For water,

$$\tilde{p}_a = B\left[\left(\frac{\tilde{\rho}_a}{\tilde{\rho}_{f0}}\right)^{\chi} - 1\right] \tag{23}$$

$$\tau_a^{\alpha\beta} = \mu\varepsilon_a^{\alpha\beta} \tag{24}$$

$$\varepsilon_a^{\alpha\beta} = \sum_{b=1}^{M}\frac{m_b}{\rho_b}v_{ba}^{\alpha}\frac{\partial W_{ab}}{\partial x_a^{\beta}} + \sum_{b=1}^{M}\frac{m_b}{\rho_b}v_{ba}^{\beta}\frac{\partial W_{ab}}{\partial x_a^{\alpha}} - \frac{2}{3}\left(\sum_{b=1}^{M}\frac{m_b}{\rho_b}\boldsymbol{v}_{ba} \cdot \nabla_a W_{ab}\right)\delta^{\alpha\beta} \tag{25}$$

where α and β denote the Cartesian components x, y, or z. $\delta^{\alpha\beta}$ is the Kronecker delta symbol. G is the shear modulus and K is the bulk modulus, respectively given by $G = \frac{E}{2\left(1+\upsilon\right)}$, $K = \frac{E}{3\left(1-2\upsilon\right)}$. E is Young's modulus and υ is the Poisson's ratio. $e_i^{\alpha\beta}$ is the deviatoric strain rate tensor, $e_i^{\alpha\beta} = \varepsilon_i^{\alpha\beta} - \frac{1}{3}\varepsilon_i^{\gamma\gamma}\delta^{\alpha\beta}$. B is a problem dependent parameter that sets a limit to maximum density variation. χ is a constant normally set to 7. $\tilde{\rho}_{f0}$ is the reference intrinsic density of water. μ is the dynamic viscosity of water.

4. Boundary contact and servo-control method

Boundary deficiency is an inherent drawback of SPH. For particles moving near or on the boundary, the support domain is incomplete and the calculated acceleration is not accurate. Several attempts have been tried in previous studies. The boundaries of rigid have been modeled using a) ghost particles, b) fluid particles, c) normalizing conditions, d) boundary particle force and e) particle-to-particle or particle-to-surface contact based on momentum equations [13] . Regrettably, the above methods can only be applied to completely smooth or rough boundary conditions. Here we adopt the frictional sliding contact algorithm proposed by Wang et al [20, 21] to simulate the contact between the mixture and boundary. The final form of the contact force is given by

$$\boldsymbol{F}_n = (1-\varsigma)\left[\frac{2m_i}{(\Delta t)^2}(d_0 + \boldsymbol{G}\cdot\boldsymbol{n})\right]\boldsymbol{n} \tag{26}$$

$$\boldsymbol{F}_\tau = \begin{cases} \dfrac{\xi|\boldsymbol{F}_n|}{|\boldsymbol{F}'_\tau|}\boldsymbol{F}'_\tau, & \text{if } |\boldsymbol{F}'_\tau| > \xi|\boldsymbol{F}_n| \\ \boldsymbol{F}'_\tau, & \text{otherwise} \end{cases} \tag{27}$$

$$\boldsymbol{F}'_\tau = \frac{2m_i}{(\Delta t)^2}(\Delta\boldsymbol{u} - \Delta\boldsymbol{u}\cdot\boldsymbol{n}) \tag{28}$$

where $\boldsymbol{F}_n$, $\boldsymbol{F}_\tau$ are the normal, tangent component of the contact force, respectively. ς defines the extent of penetration allowed and was taken as 0.01-0.1. ξ is the frictional coefficient. $\boldsymbol{G}$ is the vector from the particle to its perpendicular foot on the boundary. $\boldsymbol{n}$ is the outward normal vector of the contact surface.

Different from the single phase or quasi-single phase theory, stress boundary condition can not be applied to the mixture. It is because that the portion of the external load carried by each phase is uncertain. As shown in Fig.1, a novel method base on the above contact algorithm is developed here to simulate the stress boundary.

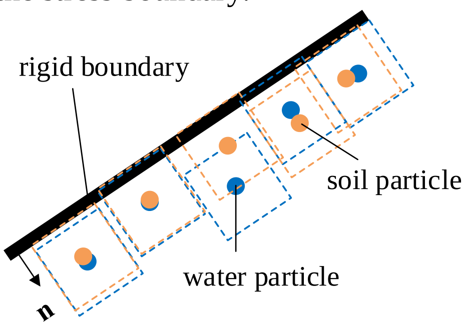

Fig.1 Schematic diagram of servo-control method

The rigid boundary is assigned velocity along the outward normal vector through

$$v_R^n = \frac{\alpha_{cs} A_{cs} \Delta t}{2\left(\sum_{i=1}^{N_s} m_i + \sum_{a=1}^{N_f} m_a\right)}(\sigma_g - \sigma_m) \tag{29}$$

$$\sigma_m = \frac{\sum_{i=1}^{N_s} F_i + \sum_{a=1}^{N_f} F_a}{A_{cs}} \tag{30}$$

where σ_g is the target stress, σ_m is the measured contact stress in the present time step; m_i and m_a represent the mass of soil and water, respectively. N_s and N_f are respectively the total number of soil and water particles contacting with the rigid. A_{cs} is the contact area. α_{cs} is a scaling factor used to weaken the oscillation, taken as 0.01. F_i and F_a are calculated through equation (26).

5. 2-D consolidation modelling and analysis

A 2-D consolidation problem was simulated to validate the two-phase mixture SPH model and the servo-control algorithm. Boer *et al*. [18] and Breuer [19] studied the same problem by FEM. The parameters used here were taken the same for comparison. The geometry of the model is shown in Fig.2. The soil-water mixture was 20.0 m long and 10.0 m wide, with $15\ \text{KPa}$ uniformly distributed load at the top. The left, right and the bottom were fixed and undrained, whereas the top was drained. The soil parameters are: $\lambda_s = 5583\ \text{KPa}$, $\mu_s = 8375\ \text{KPa}$, $\tilde{\rho}_s = 2000\ \text{kg/m}^3$, $n = 0.33$, $\upsilon = 0.2$, $k = 0.01\ \text{m/s}$. The water parameters are: $\tilde{\rho}_f = 1000\ \text{kg/m}^3$, $c_f = 97.5\ \text{m/s}$.

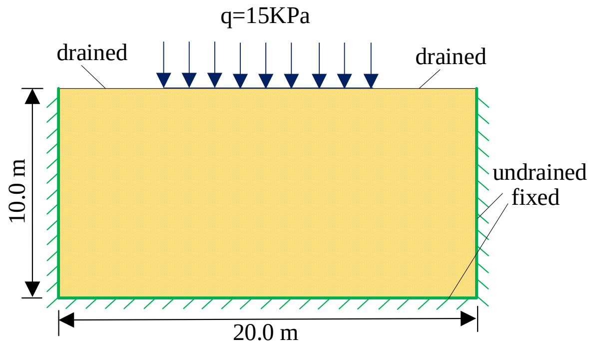

Fig.2 Geometry of the 2-D consolidation model

The initial SPH model is shown in Fig.3. Totally 800 particles were used with initial resolution $\Delta d = 0.5\ \text{m}$. The left, right and bottom were all modeled as non-slip using ghost particles. The velocity of the rigid boundary at the top was assigned velocity through equation (29) to model the stress boundary condition. Soil and water particles were initially superimposed and then moved separately according to their own governing equations.

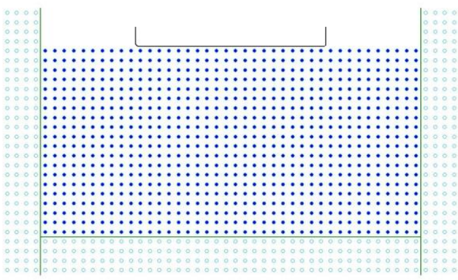

Fig.3 Initial SPH model of the 2-D consolidation problem

The evaluation of the excess pore water pressure at different intervals of time is shown in Fig.4. FEM results by Breuer [19] are also included for comparison (on the left, in KPa). It is shown that the excess pore water pressure predicted by SPH corresponds to FEM results well. In the beginning, i.e. t = 0.01 s, the excess pore water pressure increased to around 14000 Pa quickly. The reason is that the deformation of soil lagged behind the water. Accordingly, the whole external load was mainly carried by the water. With the passage of time, the pore water flew out of the void and the soil skeleton carried more and more external load. As the result, the excess pore water pressure decreased gradually. After 10 s the excess pore water pressure was about zero.

It was proved that the excess pore water pressure could be captured satisfactorily by means of the proposed method. Besides, the servo-control algorithm method could be used to simulate the stress boundary condition.

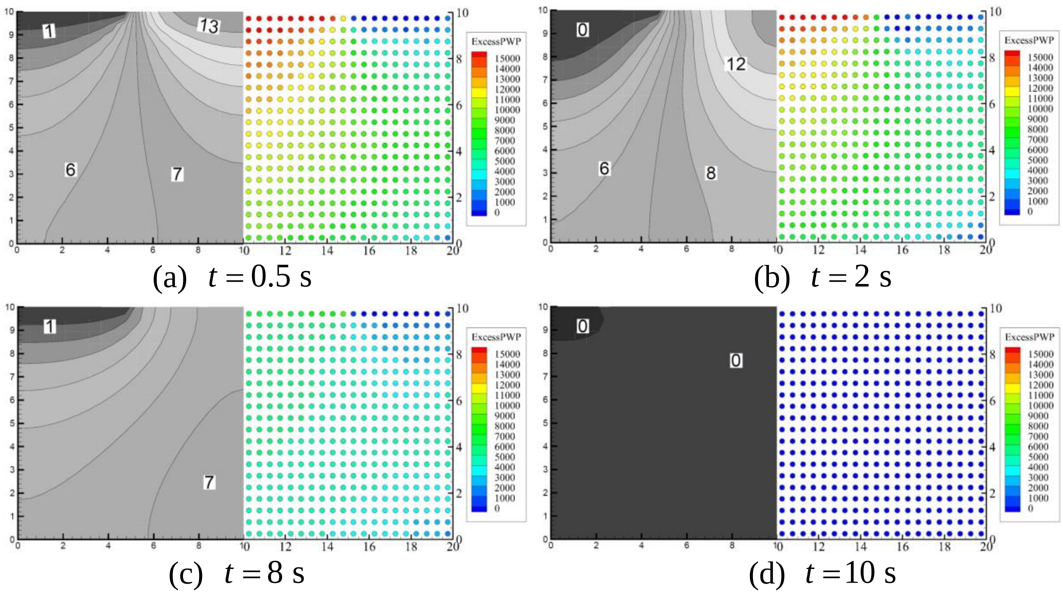

Fig 4 Comparison of excess pore water pressure between FEM (left: in KPa) and SPH (right: in Pa) at different intervals of time

6. Conclusions

The SPH based two-phase mixture model has been recently applied to geotechnical problems involving fast flow through porous media and large soil deformation. However, the applicability of the SPH based two-phase mixture model to the evaluation of pore water pressure has not been validated.

In this study, the SPH based two-phase mixture model was first improved by taking the soil porosity into account. The soil porosity was treated as a spatial variable but not a constant and was interpolated and integrated at all particles. Soil and water particles were superimposed and then moved separately according to their own governing equations. The interaction force of the two phases was composed of pore water pressure and viscous drag force. Tensile instability was properly handled by using the Monaghan's artificial pressure method. Then a servo-control method was proposed based on the frictional sliding contact algorithm in order to model the stress boundary condition. Finally, a 2-D consolidation numerical test was conducted and compared to previous research. It was proved that the SPH based two-phase mixture model could satisfactorily predict the pore water pressure. Besides, the servo-control method could model the stress boundary condition well.

Acknowledgement

This research is supported by the National Natural Science Foundation of China (Grant Nos. 51678360, 41727802 and 51779084).

References

[1] Biot MA (1956) Theory of Propagation of Elastic Waves in a Fluid-Saturated Porous Solid. I. Low-Frequency Range. J Acoust Soc Am 28:168–178 .

[2] Drew DA (1983) Mathematical Modeling of Two-Phase Flow. Annu Rev Fluid Mech 15:261–291

[3] Coussy O, Dormieux L, Detournay E (1998) From mixture theory to biot's approach for porous media. Int J Solids Struct 35:4619–4635 .

[4] Wu H, Wang J, Wang JH, Liao CC (2017) Asymmetric Adaptive Particle Refinement in SPH and Its Application in Soil Cutting Problems. Int J Comput Methods 1850052

[5] Peng C, Xu G, Wu W, et al (2017) Multiphase SPH modeling of free surface flow in porous media with variable porosity. Comput Geotech 81:239–248 .

[6] Bui HH, Sako K, Fukagawa R (2007) Numerical simulation of soil-water interaction using smoothed particle hydrodynamics (SPH) method. J Terramechanics 44:339–346 .

[7] Wang C, Wang Y, Peng C, Meng X (2016) Smoothed Particle Hydrodynamics Simulation of Water-Soil Mixture Flows. J Hydraul Eng 142:4016032 . doi: 10.1061/(ASCE)HY.1943-7900.0001163

[8] Huang Y, Zhang W, Dai Z, Xu Q (2013) Numerical simulation of flow processes in liquefied soils using a soil–water-coupled smoothed particle hydrodynamics method. Nat Hazards 69:809–827 .

[9] Maeda K, Sakai H, Sakai M (2006) Development of Seepage Failure Analysis Method of Ground With Smoothed Particle Hydrodynamics. Struct Eng / Earthq Eng 23:307s–319s .

[10] Nakamura K, Satomi T, Takahashi H (2014) Improved Model for Soil as a Two-Phase Mixture Based on Smoothed Particle Hydrodynamics (SPH). 1053–1060

[11] Liu MB, Liu GR, Zong Z (2008) An overview of smoothed particle hydrodynamics. 1:135–188

[12] Liu MB, Shao J, Chang J (2012) On the treatment of solid boundary in smoothed particle hydrodynamics. Sci China Technol Sci 55:244–254 .

[13] Monaghan JJ, Kajtar JB (2009) SPH particle boundary forces for arbitrary boundaries. Comput Phys Commun 180:1811–1820 .

[14] Wendland H (1995) Piecewise polynomial, positive definite and compactly supported radial functions of minimal degree. Adv Comput Math 4:389–396 .

[15] Antuono M, Colagrossi A, Marrone S, Molteni D (2010) Free-surface flows solved by means of SPH schemes with numerical diffusive terms. Comput Phys Commun 181:532–549 .

[16] Monaghan JJ (1995) SPH simulation of multi- phase flow. Comput Phys Commun 87:1–2

[17] Monaghan JJ (2000) SPH without a Tensile Instability. J Comput Phys 159:290–311 .

[18] Boer R, Ehlers W, Liu Z (1993) One-dimensional transient wave propagation in fluid-saturated incompressible porous media. Arch Appl Mech 63:59–72 . doi: 10.1007/BF00787910

[19] Breuer S (1999) Quasi-Static and Dynamic Behavior of Saturated Porous Media with Incompressible Constituents. Transp Porous Media 34:285–303 .

[20] Wang J, Wu H, Gu C, Hua H (2013) Simulating frictional contact in smoothed particle hydrodynamics. Sci China Technol Sci 56:1779–1789 .

[21] Wang J, Chan D (2014) Frictional contact algorithms in SPH for the simulation of soil-structure interaction. Int J Numer Anal Methods Geomech 38:747–770 .